AGU PUBLICATIONS

Geophysical Research Letters

RESEARCH LETTER
10.1002/2014GL059653

Key Points:
- Process-dependent trapping
- Effective gas barrier through degassing process
- Management of subsurface flow processes

Correspondence to:
L. Zuo,
linzuo@stanford.edu

Citation:
Zuo, L., and S. M. Benson (2014), Process-dependent residual trapping of CO_2 in sandstone, *Geophys. Res. Lett.*, *41*, 2820–2826, doi:10.1002/2014GL059653.

Received 19 FEB 2014
Accepted 8 APR 2014
Accepted article online 10 APR 2014
Published online 24 APR 2014

Process-dependent residual trapping of CO_2 in sandstone

Lin Zuo[1] and Sally M. Benson[1]

[1]Department of Energy Resources Engineering, Stanford University, Stanford, California, USA

Abstract This paper demonstrates that the nature and extent of residual CO_2 trapping depend on the process by which the CO_2 phase is introduced into the rock. We compare residual trapping of CO_2 in Berea Sandstone by imbibing water into a core containing either exsolved CO_2 or CO_2 introduced by drainage. X-ray computed tomography measurements are used to map the spatial distribution of CO_2 preimbibition and postimbibition. Unlike during drainage where the CO_2 distribution is strongly influenced by the heterogeneity of the rock, the distribution of exsolved CO_2 is comparatively uniform. Postimbibition, the CO_2 distribution retained the essential features for both the exsolved and drainage cases, but twice as much residual trapping is observed for exsolved CO_2 even with similar preimbibition gas saturations. Residually trapped exsolved gas also disproportionately reduced water relative permeability. Development of process-dependent parameterization will help better manage subsurface flow processes and unlock benefits from gas exsolution.

1. Introduction

Geological storage projects would introduce millions of tons of CO_2 into deep underground formations resulting in complex flow and transport processes operating over millennial timescales [*Metz et al.*, 2005]. Initially, flow and transport of CO_2 will be dominated by multiphase displacements of in situ fluids [*Pruess and Garcia*, 2002; *Nordbotten et al.*, 2005]. Over time and with distance from the injection well, a progressively larger fraction of the CO_2 will dissolve into reservoir brines due to postinjection gravitational equilibration [*Hesse et al.*, 2008; *Doughty and Pruess*, 2004] and convective mixing [*Riaz et al.*, 2006]. Up to 5% mass fraction of CO_2 can dissolve into reservoir brines depending on pressure, temperature, and brine composition [*Duan and Sun*, 2003]. Exsolution of dissolved CO_2 occurs when pore pressures decline [*Enouy et al.*, 2011; *Zuo et al.*, 2012, 2013] or temperatures rise [*Luhmann et al.*, 2012], resulting in the formation of a separate CO_2 phase. For example, if CO_2-saturated brine migrates upward through faults, leaking boreholes or seals, a separate phase of CO_2 exsolves as the pressure decreases [*Falta et al.*, 2013; *Oldenburg et al.*, 2012]. Exsolution can also occur during CO_2-enhanced oil recovery, particularly near the production wells [*Alizadeh et al.*, 2011] and can improve secondary recovery when exsolved CO_2 blocks water flow paths, displacing water into oil-filled pores and mobilizes residual oil [*Zuo and Benson*, 2013].

Numerical simulations using discretized mass and energy balance equations are commonly used to predict the influence of these complex processes on the long-term fate of CO_2 or on the ultimate recovery from an oilfield [*Oldenburg et al.*, 2001; *Kumar et al.*, 2004]. Key inputs include relative permeability and capillary pressure characteristic curves and trapping coefficients. These characteristic curves are typically treated as single-valued functions of the saturation, or in some cases include hysteresis, or history-dependent values [*Juanes et al.*, 2006; *Doughty*, 2007; *Altundas et al.*, 2011]. Implicitly, these models assume that characteristic curves are not a function of the process by which a secondary phase is introduced into the rock, for example, by drainage in the cases of CO_2 injection or by exsolution, in the case of declining pressures.

Differences in the spatial distribution of CO_2 are expected to result from the process by which separate phase CO_2 is introduced into the rock. For example, during drainage, subcore-scale heterogeneity has a strong influence in the spatial distribution and transport of CO_2 [*Chaouche et al.*, 1994; *Perrin and Benson*, 2010; *Shi et al.*, 2011]. Capillary heterogeneity creates barriers that prevent CO_2 from entering portions of the rock with high capillary entry pressure [*Ferrand and Celia*, 1992; *Ringrose et al.*, 1993; *Illangasekare et al.*, 1995; *Krevor et al.*, 2011; *Shi et al.*, 2011; *Krause et al.*, 2011]. After the initial pore invasion when saturations are no longer changing, the drainage-induced gas distribution behind the invasion front is at local

capillary equilibrium [*Leverett*, 1941; *Lenormand et al*., 1983; *Blunt et al*., 2002], although nonequilibrium capillarity effects are observed during initial invasion [*Barenblatt et al*., 2003; *Berg et al*., 2013]. Imbibition following drainage will displace some of the CO_2 but trap the rest as disconnected ganglia that show strong dependence on the topology of the nonwetting fluid, wettability, and pore geometries [*Chaudhary et al*., 2013; *Joekar-Niasar et al*., 2013; *Kim et al*., 2012; *Tanino and Blunt*, 2012: *Tokunaga et al*., 2013]. Pore-scale imaging of postdrainage trapping shows that trapped supercritical CO_2 in a water-wet system yields a power law cluster size distribution [*Andrew et al*., 2013], as predicted from percolation theory [*Lorenz and Ziff*, 1998], and capillary heterogeneity has been shown to increase trapping [*Krevor et al*., 2011; *Saadatpoor et al*., 2010].

In contrast to drainage, an exsolved CO_2 phase consists primarily of disconnected rather than pore-spanning bubbles that are uniformly distributed throughout the rock and not strongly influenced by capillary heterogeneity [*Luhmann et al*., 2012; *Zuo et al*., 2013]. The capillary pressure in each bubble is determined by local pore geometry and consequently can vary throughout the rock. Liberation of gas has been found to significantly reduce both gas and liquid mobility in gas-oil systems [*Fishlock et al*., 1988; *Grattoni et al*., 1998; *Naylor et al*., 2000; *Tang and Firoozabadi*, 2003] and in CO_2-water system [*Zuo et al*., 2012] under high pressures while *Fry et al*. [1997], *Zhao and Ioannidis* [2011], and *Enouy et al*. [2011] show that water during exsolution at near-ambient conditions is as mobile as during drainage, and exsolved air/CO_2 is mobilized by capillary instability and buoyancy forces. So far, there has been no explanation for this discrepancy. Nucleation and postnucleation processes that control the distribution and morphology of exsolved gas in the pore space depend on rock types, fluid properties, and pressure conditions [*Li and Yortsos*, 1995]. In light of the disconnected nature of the gas phase following exsolution [*Zuo et al*., 2013], we hypothesize that under reservoir conditions, postexsolution residual gas trapping will be different than postdrainage trapping and require process-specific parameterization of the residual trapping coefficient and relative permeability.

In this paper, we compare postdrainage and postexsolution CO_2/water trapping under the same pressure and temperature conditions. Preimbibition and postimbibition gas distributions are compared and quantitatively analyzed. Relative permeabilities at imbibition endpoints are also measured to demonstrate the process dependency and influence of gas morphology on multiphase flow properties.

2. Experimental Methods

2.1. Materials and Equipment

For the experiments we use a core of Berea Sandstone obtained from a commercial quarry (Cleveland Quarries), 15 cm in length and 5 cm in diameter. The core is heated at 700°C overnight to stabilize swelling clays before the experiments. The core-flooding apparatus is similar to the setup described by *Perrin and Benson* [2010]. Five syringe pumps (Teledyne Isco, model 500D and 1000D) are used to circulate fluids at elevated pressure and temperature in a closed loop. The core is placed in an aluminum core holder, and an X-ray computed tomography scanner (General Electric HiSpeed CT/i) is used to obtain rock porosity and phase saturations (500 μm pixel resolution in cross sections; 1 mm interval in length) during the experiments [*Akin and Kovscek*, 2003]. Deionized water and CO_2 are used as wetting and nonwetting phases.

2.2. Procedure

The rock is scanned sequentially while air filled (atmosphere pressure), CO_2 filled (4.14 MPa), water filled (4.14 MPa), and equilibrated carbonated water filled (4.14 MPa) to calculate rock porosity (Figure 1a) and obtain background scans of the core. All reported X-ray CT data are the average of two replicate scans. Absolute permeability of the core, 507 mD, is measured when the core is water filled. The core and injected fluids are maintained at 50°C throughout experiments. A 2.76 MPa confining pressure is applied to the core.

The drainage process is started by coinjecting CO_2 at 9 mL/min and carbonated water at 1 mL/min into the core at 4.14 MPa. Multiple scans are taken to measure the CO_2 saturation distribution and determine when it stabilizes. CO_2 injection is stopped when the CO_2 saturation distribution stabilized. An imbibition process follows immediately by injecting carbonated water at 1 mL/min. Multiple scans are taken until the residual gas saturation is reached. After the gas saturation stabilizes at 1 mL/min, the carbonated water injection rate

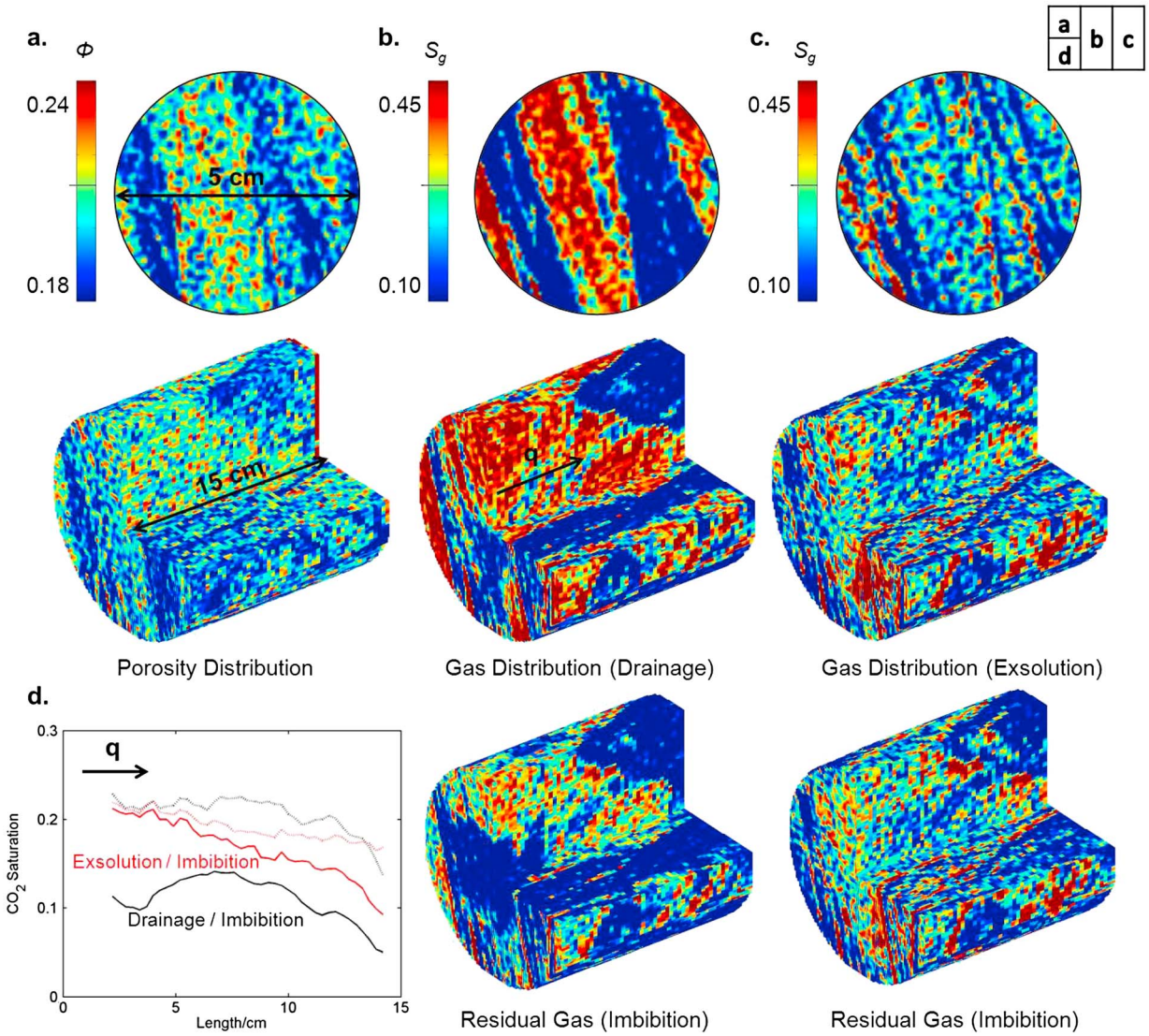

Figure 1. Porosity distributions of the (a) middle cross section and the whole core, (b) corresponding CO_2 saturation distributions in drainage/imbibition and (c) exsolution/imbibition, and (d) cross section CO_2 saturation profiles.

is then increased to 5 and then 15 mL/min. After the gas saturation stabilized at each flow rate, the relative permeability to the aqueous phase is measured.

For the exsolution process, the core is fully saturated with carbonated water equilibrated at 10.34 MPa. Afterward, the upstream end of the core is sealed, and the downstream is regulated at a constant pressure decline rate of 0.1 or 1 MPa/h until the pore pressure is reduced to 4.14 MPa and held constant thereafter at 50°C. The pressure/temperature conditions simulate an upward migration of carbonated brine from a designated storage reservoir around 1000 m to a shallower depth around 400 m which is typical for CO_2 storage projects. Small pressure gradients are observed across the core during depressurization, and this is similar to the condition when exsolution occurs in a reservoir, although the pressure decline rates are expedited. While rate-dependent behaviors of exsolved gas have been observed with hydrocarbons [*Scherpenisse et al.*, 1994], no significant difference in gas aggregation/trapping are observed in our experiments between 0.1 and 1 MPa/h pressure decline rates. Results discussed here are for a pressure decline rate of 1 MPa/h. Identical to the drainage/imbibition experiment, following exsolution, sequential imbibition at 1, 5, and 15 mL/min with carbonated water (equilibrated at 4.14 MP) injections are conducted. The injection rate is adjusted after the CO_2 saturation stabilizes.

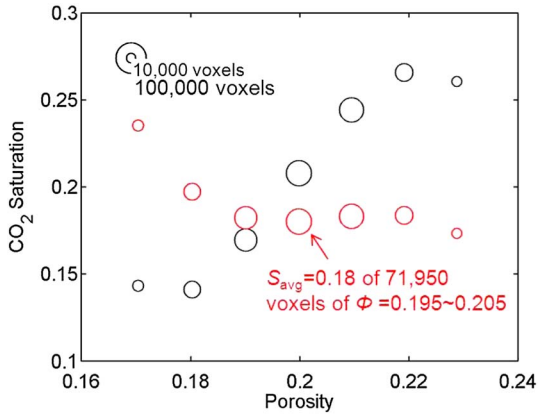

Figure 2. Porosity saturation correlations for drainage (black) and exsolution (red). Saturations are average values over voxels within porosity intervals (0.01 width). Circle area represents the number of voxels within the particular porosity interval.

3. Results

Figure 1 shows the middle cross section and the whole core's porosity distributions (Figure 1a), CO_2 distributions in drainage/imbibition process (Figure 1b), and exsolution/imbibition process (Figure 1c). Cross-sectional averaged CO_2 saturation profiles are shown in Figure 1d (black dotted/solid curves: drainage/imbibition; red dotted/solid curves: exsolution/imbibition). Residual gas saturations for both scenarios shown are equilibrated at 15 mL/min carbonated water injection. The core has an average porosity of 0.20, and alternating low- and high-porosity zones appear as high-angle bedding planes along the length of the core. This feature affected the drainage CO_2 saturation distribution significantly and manifested the importance of small-scale capillary heterogeneity on nonwetting phase distribution in drainage. High-porosity regions have significantly higher CO_2 saturations than regions with just several percent lower porosity. In contrast with drainage, CO_2 exsolution is less affected by the capillary heterogeneity, and CO_2 is distributed more evenly, although the influence of bedding structures on the saturation distribution is still somewhat evident. Overall, the whole core has similar average CO_2 saturations in both cases, 0.20 and 0.18 for drainage and exsolution, respectively.

Figure 2 illustrates clear statistical differences between the saturation distribution for the exsolution and drainage cases. There is a positive correlation between drainage CO_2 saturation and porosity while the exsolution CO_2 saturation is independent of porosity. The area of circle represents the number of voxels of the whole core within a certain porosity interval. For example, the red circle centered at 0.20 porosity and 0.18 saturation shows that the average CO_2 saturation is 0.18 for all voxels with porosity 0.20 ± 0.005 (71,950 individual voxels). The standard deviation of each aggregation of drainage CO_2 saturation is ~14% and ~10% in exsolution CO_2 saturation. This large spread is primarily caused by small-scale heterogeneity and sedimentary structures.

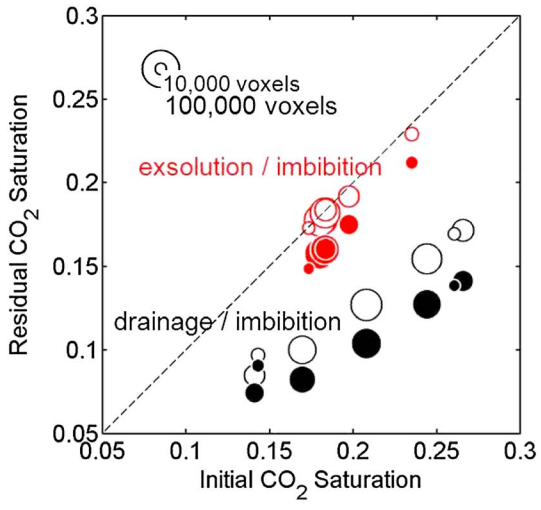

Figure 3. Residual CO_2 saturations versus the initial CO_2 saturations in drainage/imbibition (black) and exsolution/ imbibition (red). Unit slope is plotted in dashed line. Residual CO_2 saturations after 1 and 15 mL/min carbonated water injection are in open and filled circles.

Figure 3 shows residual CO_2 saturations after 1 and 15 mL/min carbonated water injections versus the initial CO_2 saturations. Data points are the aggregation of voxels defined identically in Figure 2. Similar to previous studies [*Pentland et al.*, 2011; *Krevor et al.*, 2012], in a water-wet system, the residual CO_2 saturation increases monotonically with the initial CO_2 saturation in all four cases. However, capillary trapping is much more extensive with exsolved gas. This sole explanation for this difference must stem from the differences in gas morphology, because the interfacial tension between CO_2 and water is the same for both experiments. Figure 4 shows corresponding Land trapping coefficients, $C = \frac{1}{S_{gr}} - \frac{1}{S_{gi}}$, for postdrainage and postexolution imbibition [*Land*, 1968], where S_{gi} and S_{gr} are initial and residual gas saturations. During carbonated water injection at 1 mL/min, almost all exsolved gas is immobile, and the curve

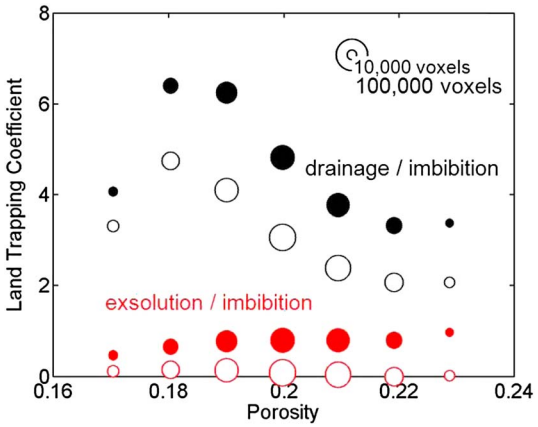

Figure 4. Land coefficients [*Land*, 1968] in drainage/imbibition (black) and exsolution/imbibition (red). Coefficients of 1 and 15 mL/min carbonated water injection are marked in open and filled circles.

overlaps with the unit slop line (Figure 3), indicating a near-zero Land coefficient (Figure 4). At an injection rate of 15 mL/min, the average Land coefficient increases to 1, showing that at higher injection rates viscous forces can overcome capillary forces in some locations to mobilize a small portion of previously trapped gas. Rate-dependent residual trapping is also observed for drainage gas, but overall, capillary trapping is weaker. Different from exsolved gas, which has similar Land coefficients over the range of initial saturation, drainage gas has larger Land coefficients (4.7 and 6.5 at 1 and 15 mL/min injections) in low-porosity regions and smaller Land coefficients (2.1 and 3.5 at 1 and 15 mL/min injections) in high-porosity regions. This suggests stronger capillary trapping in high-porosity regions of the rock tested here. However, increased trapping in high-porosity regions could actually be the consequence of downstream capillary barriers [*Krevor et al.*, 2011] and sedimentary structures which lead to bypass during imbibition [*Huang et al.*, 1995].

4. Discussion

Injection of CO_2 at low capillary numbers (10^{-8}–10^{-7}) leads to strongly capillary heterogeneity controlled gas distribution during drainage. Capillary equilibrium contributes to the large gas saturation contrast observed (Figure 1b) between neighboring regions. On the contrary, gas exsolved almost uniformly in all porosity regions (Figure 2) which indicates this in situ gas evolution is not hindered by capillary heterogeneity, at least over the range of pore sizes relevant here (10–100 μm pore radius in Berea Sandstone).

During imbibition, almost all exsolved gas ($S_{gr} = 0.18$) is trapped, and only a small fraction is mobilized ($S_{gr} = 0.16$) when the water injection rate increases from 1 ($Ca \sim 10^{-7}$) to 15 ($Ca \sim 10^{-6}$) mL/min. In contrast, the postdrainage gas saturation decreases from 0.2 to 0.12 during 1 mL/min water injection and further down to 0.10 during 15 mL/min injection. These observations can be explained by the morphology of the exsolved CO_2. Bubbles nucleate instantaneously under large supersaturation [*Firoozabadi and Kashchiev*, 1996] and distribute uniformly in the core. Individual bubbles grow by diffusion from the aqueous phase into the gas phase. As the bubble grows, capillary pressure will increase when the gas-liquid interface penetrates into pore throats. When the capillary threshold at the throats is overcome, the bubble will expand into neighboring pores. Due to the high CO_2/water interfacial tension, the gas-liquid interface requires high energy to span multiple pores, and capillarity instability in high-aspect ratio pores leads to snap off [*Roof*, 1970]. A dispersed, residual phase-like morphology is formed as CO_2 evolves in porous media and becomes trapped in pores [*Zuo et al.*, 2013].

The unique morphology of exsolved gas exhibits both opportunities and challenges in management of subsurface flow processes. In geological carbon storage, seals with low permeabilities and high capillary entry pressures are expected to prevent gas or supercritical phase CO_2 from leaking out of the storage reservoir. However, the seal does not prevent dissolved CO_2 from migrating upward. If a dissolved phase migrates into the seal and a gas phase exsolves due to depressurization, the mobility of the aqueous phase will be further reduced, thus suppressing further aqueous phase migration [*Falta et al.*, 2013]. This CO_2 gas barrier can also be manipulated for water conformance and mobility control in oil/gas applications [*Zuo et al.*, 2013]. By decreasing the reservoir pressure, CO_2 exsolves as a secondary residual phase in addition to trapped oil. A highly dispersed morphology and a strong nonwetting character of the CO_2 phase would promise an effective block of the water flow therefore improving sweep efficiency.

In the experiments, water relative permeability is measured at the end of imbibition process at 15 mL/min (~10 m/d), which is higher than normal flow rates under reservoir conditions. The water relative permeability

at the imbibition endpoint is: $k_{rw} = 0.28$ at $S_{gr} = 0.16$ in postexsolution imbibition and $k_{rw} = 0.65$ at $S_{gr} = 0.10$ in postdrainage imbibition, with similar initial CO_2 saturations (drainage: 0.20; exsolution: 0.18). This parameterization discrepancy, along with different trapping coefficients, is not reflected in reservoir simulators today. It is clear that not only history-dependent behavior (hysteresis) but also process-dependent behavior will result in very different multiphase flow parameters. Poorly interconnected exsolved gas interferes more strongly with the water flow than injected gas, even at the very high flow rates tested here. For the CO_2-brine system, at high pressures and in consolidated rocks, using postdrainage imbibition relative permeability parameterizations for simulations involving exsolution will lead to overestimation of gas and liquid phase flows. The large mobility reduction of the CO_2 and water observed here is consistent with results of exsolution associated with drainage in different sandstones studied previously [*Zuo et al.*, 2012].

Consequently, the challenge that lies ahead is the need to distinguish and account for process-specific parameterizations of key inputs such as relative permeability and trapping coefficients. For a simulation involving only one of the processes, the solution can be straightforward, as long as the appropriate process-specific parameterization is included. However, in general, it is possible that multiple processes are acting concurrently in different portions of the subsurface, and multiple parameterizations are required. Tracking both history-dependent and processes-dependent phenomenon will be required for accurate simulation. Development of process-dependent parameterization will help better manage subsurface flow processes and unlock benefits from gas exsolution.

Acknowledgments

We thank the Global Climate and Energy Project at Stanford University for funding this research. Readers can access the data from this paper for free by contacting the authors.

The Editor thanks two anonymous reviewers for their assistance in evaluating this paper.

References

Akin, S., and A. R. Kovscek (2003), Computed tomography in petroleum engineering research, in *Applications of X-Ray Computed Tomography in the Geosciences*, vol. 215, edited by S. Akin and A. R. Kovscek, pp. 23–38, The Geol. Soc. London, London, U. K.

Alizadeh, A. H., M. A. Ioannidis, and M. Piri (2011), CO_2-saturated brine flooding: An effective process for mobilization and recovery of waterflood residual oil. Presented at the International Symposium of the Society of Core Analysts, Austin, Tex., 18–21 Sept.

Altundas, Y. B., T. S. Ramakrishnan, N. Chugunov, and R. de Louebens (2011), Retardation of CO_2 caused by capillary pressure hysteresis: A new CO_2 trapping mechanism, *SPE J.*, *16*(4), 784–794.

Andrew, M., B. Bijeljic, and M. J. Blunt (2013), Pore-scale imaging of geological carbon dioxide storage under in situ conditions, *Geophys. Res. Lett.*, *40*, 3915–3918, doi:10.1002/grl.50771.

Barenblatt, G. I., T. W. Patzek, and D. B. Silin (2003), The mathematical model of non-equilibrium effects in water–oil displacement, *SPE J.*, *8*(4), 409–416.

Berg, S., et al. (2013), Real-time 3D imaging of Haines jumps in porous media flow, *Proc. Natl. Acad. Sci. U.S.A.*, *110*(10), 3755–3759.

Blunt, M. J., M. D. Jackson, M. Piri, and P. H. Valvatne (2002), Detailed physics, predictive capabilities and macroscopic consequences for pore-network models of multiphase flow, *Adv. Water Res.*, *25*(8), 1069–1089.

Chaouche, M., N. Rakotomalala, D. Salin, B. Xu, and Y. Yortsos (1994), Capillary effects in drainage in heterogeneous porous media: Continuum modelling, experiments and pore network simulations, *Chem. Eng. Sci.*, *49*(15), 2447–2466.

Chaudhary, K., M. Bayani Cardenas, W. W. Wolfe, J. A. Maisano, R. A. Ketcham, and P. C. Bennett (2013), Pore-scale trapping of supercritical CO_2 and the role of grain wettability and shape, *Geophys. Res. Lett.*, *40*, 3878–3882, doi:10.1002/grl.50658.

Doughty, C. (2007), Modeling geologic storage of carbon dioxide: Comparison of non-hysteretic and hysteretic characteristic curves, *Energy Convers. Manage.*, *48*, 1768–1781.

Doughty, C., and K. Pruess (2004), Modeling supercritical carbon dioxide injection in heterogeneous porous media, *Vadose Zone J.*, *3*, 837–847.

Duan, Z., and R. Sun (2003), An improved model calculating CO_2 solubility in pure water and aqueous NaCl solutions from 273 to 533 K and from 0 to 2000 bar, *Chem. Geol.*, *193*(3), 257–271.

Enouy, R., M. Li, M. A. Ioannidis, and A. Unger (2011), Gas exsolution and flow during supersaturated water injection in porous media: II. Column experiments and continuum modeling, *Adv. Water Resour.*, *34*(1), 15–25.

Falta, R., L. Zuo, and S. M. Benson (2013), Migration of exsolved CO_2 following depressurization of saturated brines, *J. Greenhouse Gas. Sci. Technol.*, *3*(6), 503–515.

Ferrand, L. A., and M. A. Celia (1992), The effect of heterogeneity on the drainage capillary pressure-saturation relation, *Water Resour. Res.*, *28*(3), 859–870, doi:10.1029/91WR02679.

Firoozabadi, A., and D. Kashchiev (1996), Pressure and volume evolution during gas phase formation in solution gas drive process, *SPE J.*, *1*(3), 219–223.

Fishlock, T. P., R. A. Smith, B. M. Soper, and R. W. Wood (1988), Experimental studies on the waterflood residual gas saturation and its production by blowdown, *SPE Reservoir Eng.*, *3*(2), 387–394.

Fry, V. A., J. S. Selker, and S. M. Gorelick (1997), Experimental investigations for trapping oxygen gas in saturated porous media for in situ bioremediation, *Water Resour. Res.*, *33*(12), 2687–2696, doi:10.1029/97WR02428.

Grattoni, C. A., R. I. Hawes, and R. A. Dawe (1998), Relative permeabilities for the production of solution gas from waterflooded residual oil, In International Symposium of the Society of Core Analysts, The Hague, Netherlands, 14–16 Sept.

Hesse, M. A., F. M. Orr, and H. A. Tchelepi (2008), Gravity currents with residual trapping, *J. Fluid Mech.*, *611*, 35–60.

Huang, Y., P. Ringrose, and K. S. Sorbie (1995), Capillary trapping mechanisms in water-wet laminated rocks, *SPE Reservoir Eng.*, *10*(4), 287–292.

Illangasekare, T. H., J. L. Ramsey, K. H. Jensen, and M. B. Butts (1995), Experimental study of movement and distribution of dense organic contaminants in heterogeneous aquifers, *J. Contam. Hydrol.*, *20*, 1–25.

Juanes, R., E. J. Spiteri, F. M. Orr, and M. J. Blunt (2006), Impact of relative permeability hysteresis on geological CO_2 storage, *Water Resour. Res.*, *42*, W12418, doi:10.1029/2005WR004806.

Kim, Y., J. Wan, T. J. Kneafsey, and T. K. Tokunaga (2012), Dewetting of silica surfaces upon reactions with supercritical CO_2 and brine: Pore-scale studies in micromodels, *Environ. Sci. Technol.*, *46*(7), 4228–4235.
Joekar-Niasar, V., F. Doster, R. T. Armstrong, D. Wildenschild, and M. A. Celia (2013), Trapping and hysteresis in two-phase flow in porous media: A pore-network study, *Water Resour. Res.*, *49*, 4244–4256, doi:10.1002/wrcr.20313.
Krause, M., J. C. Perrin, and S. M. Benson (2011), Modeling permeability distributions in a sandstone core for history matching coreflood experiments, *SPE J.*, *16*(4), 768–777.
Krevor, S. C. M., R. Pini, B. Li, and S. M. Benson (2011), Capillary heterogeneity trapping of CO_2 in a sandstone rock at reservoir conditions, *Geophys. Res. Lett.*, *38*, L15401, doi:10.1029/2011GL048239.
Krevor, S. C. M., R. Pini, L. Zuo, and S. M. Benson (2012), Relative permeability and trapping of CO_2 and water in sandstone rocks at reservoir conditions, *Water Resour. Res.*, *48*, W02532, doi:10.1029/2011WR010859.
Kumar, A., M. Noh, G. A. Pope, K. Sepehrnoori, S. Bryant and L. W. Lake (2004), Reservoir simulation of CO_2 storage in deep saline aquifers, SPE-89343-MS, In SPE/DOE Symposium on Improved Oil Recovery, Tulsa, Okla., 17–21 April.
Land, C. S. (1968), Calculation of imbibition relative permeability for two and three-phase flow from rock properties, *SPE J.*, *8*(2), 149–156.
Lenormand, R., C. Zarcone, and A. Sarr (1983), Mechanisms of the displacement of one fluid by another in a network of capillary ducts, *J. Fluid Mech.*, *135*(34), 337–353.
Leverett, M. C. (1941), Capillary behavior in porous solids, *Trans. Soc. Petrol. Eng. AIME*, *142*, 152–169.
Li, X., and Y. C. Yortsos (1995), Theory of multiple bubble growth in porous media by solute diffusion, *Chem. Eng. Sci.*, *50*(8), 1247–1271.
Lorenz, C. D., and R. M. Ziff (1998), Precise determination of the bond percolation thresholds and finite-size scaling corrections for the sc, fcc and bcc lattices, *Phys. Rev. E*, *57*(1), 230–236.
Luhmann, A. J., X. Z. Kong, B. M. Tutolo, K. Ding, M. O. Saar, and W. E. Seyfried Jr. (2012), Permeability reduction produced by grain reorganization and accumulation of exsolved CO_2 during geologic carbon sequestration: A new CO_2 trapping mechanism, *Environ. Sci. Technol.*, *47*(1), 242–251.
Metz, B., O. Davidson, H. C. De Coninck, M. Loos, and L. A. Meyer (2005), *IPCC Special Report on Carbon Dioxide Capture and Storage: Prepared by Working Group III of the Intergovernmental Panel on Climate Change*, pp. 442, IPCC, Cambridge Univ. Press, Cambridge, U. K., and New York.
Naylor, P., T. Fishlock, D. Mogford, and R. Smith (2000), Relative permeability measurements for post-waterflood depressurisation of the Miller field, North Sea, In SPE Annual Technical and Exhibition, Dallas, Tex., 1–4 Oct.
Nordbotten, J. M., M. A. Celia, and S. Bachu (2005), Injection and storage of CO_2 in deep saline aquifers: Analytical solution for CO_2 plume evolution during injection, *Transp. Porous Media*, *58*(3), 339–360.
Oldenburg, C. M., K. Pruess, and S. M. Benson (2001), Process modeling of CO_2 injection into natural gas reservoirs for carbon sequestration and enhanced gas recovery, *Energy Fuels*, *15*(2), 293–298.
Oldenburg, C. M., C. Doughty, C. A. Peters, and P. F. Dobson (2012), Simulations of long-column flow experiments related to geologic carbon sequestration: Effects of outer wall boundary condition on upward flow and formation of liquid CO_2, *Greenhouse Gas Sci. Technol.*, *2*(4), 279–303.
Pentland, C. H., R. El-Maghraby, S. Iglauer, and M. J. Blunt (2011), Measurements of the capillary trapping of super-critical carbon dioxide in Berea sandstone, *Geophys. Res. Lett.*, *38*, L06401, doi:10.1029/2011GL046683.
Perrin, J. C., and S. M. Benson (2010), An experimental study on the influence of sub-core scale heterogeneities on CO_2 distribution in reservoir rocks, *Transp. Porous Media*, *82*(1), 93–109.
Pruess, K., and J. Garcia (2002), Multiphase flow dynamics during CO_2 disposal into saline aquifers, *Environ. Geol.*, *42*(2–3), 282–295.
Riaz, A., M. A. Hesse, H. A. Tchelepi, and F. M. Orr (2006), Onset of convection in a gravitationally unstable diffusive boundary layer in porous media, *J. Fluid Mech.*, *548*, 87–111.
Ringrose, P., K. S. Sorbie, P. Corbett, and J. Jensen (1993), Immiscible flow behaviour in laminated and cross-bedded sandstones, *J. Pet. Sci. Eng.*, *9*(2), 103–124.
Roof, J. G. (1970), Snap-off of oil droplets in water-wet pores, *Old SPE J.*, *10*(1), 85–90.
Saadatpoor, E., S. L. Bryant, and K. Sepehrnoori (2010), New trapping mechanism in carbon sequestration, *Transp. Porous Media*, *82*(1), 3–17.
Scherpenisse, W., K. Wit, A. E. Zweers, G. Shoei, and V. Avend (1994), Predicting gas saturation buildup during depressurisation of a North Sea oil reservoir, SPE-28842-MS, In European Petroleum Conference, London, U. K., 25–27 Oct.
Shi, J. Q., Z. Xue, and S. Durucan (2011), Supercritical CO_2 core flooding and imbibition in Tako sandstone—Influence of sub-core scale heterogeneity, *Int. J. Greenhouse Gas Control*, *5*(1), 75–87.
Tang, G. Q., and A. Firoozabadi (2003), Gas- and liquid-phase relative permeabilities for cold production from heavy oil reservoir, *SPE Reservoir Eval. Eng.*, *6*(2), 70–80.
Tanino, Y., and M. J. Blunt (2012), Capillary trapping in sandstones and carbonates: Dependence on pore structure, *Water Resour. Res.*, *48*, W08525, doi:10.1029/2011WR011712.
Tokunaga, T. K., J. Wan, J. W. Jung, T. W. Kim, Y. Kim, and W. Dong (2013), Capillary pressure and saturation relations for supercritical CO_2 and brine in sand: High-pressure Pc(Sw) controller/meter measurements and capillary scaling predictions, *Water Resour. Res.*, *49*, 4566–4579, doi:10.1002/wrcr.20316.
Zhao, W., and M. A. Ioannidis (2011), Gas exsolution and flow during supersaturated water injection in porous media: I. Pore network modeling, *Adv. Water Resour.*, *34*(1), 2–14.
Zuo, L., S. C. M. Krevor, R. W. Falta, and S. M. Benson (2012), An experimental study of CO_2 exsolution and relative permeability measurements during CO_2 saturated water depressurization, *Transp. Porous Media*, *91*(2), 459–478.
Zuo, L., C. Zhang, R. W. Falta, and S. M. Benson (2013), Micromodel investigations of CO_2 exsolution from carbonated water in sedimentary rocks, *Adv. Water Res.*, *53*, 188–197.
Zuo, L., and S. M. Benson (2013), Exsolution enhanced oil recovery with concurrent CO_2 sequestration, *Energy Procedia*, *37*, 6957–6963.